

Clinical research device for ovarian cancer detection by optical spectroscopy in the ultraviolet C-visible

Ronie George

University of Arizona
College of Optical Sciences
1630 East University Boulevard
Tucson, Arizona 85724

Archana Chandrasekaran

University of Arizona
Department of Electrical and Computer Engineering
1230 East Speedway Boulevard
Tucson, Arizona 85721

Molly A. Brewer

University of Connecticut
Neag Comprehensive Cancer Center
263 Farmington Avenue
Farmington, Connecticut 06030

Kenneth D. Hatch

University of Arizona
Department of Obstetrics and Gynecology
1501 North Campbell Avenue
Tucson, Arizona 85724

Urs Utzinger

University of Arizona
Biomedical Engineering Department
1127 East James E. Rogers Way
Tucson, Arizona 85721

1 Introduction

Ovarian cancer has the highest mortality rate of all gynecological cancers.¹⁻³ In 2009, it was the fifth leading cause of cancer-related death among U.S. women, and 21,550 new cases and 14,600 deaths were projected.³ When detected in late stage (e.g., III-IV), five-year survival is low (5 to 15%), but when disease is confined to the ovaries, five-year survival is 80 to 90% supporting the need for early detection. The major obstacles in developing an early detection protocol for ovarian cancer are an undefined premalignant lesion, a potential for early metastasis,⁴ poor access to the ovaries, inaccurate screening technologies, and the tendency of the disease to be asymptomatic in the early stages.

Ninety percent of ovarian cancers originate from the surface epithelium^{5,6} of either the ovary or the fallopian tube, and the more aggressive of these cancers may metastasize very early to the peritoneal cavity. Early diagnosis, while the disease is still localized at its origin, results in higher cure rates, as it provides the physician with more treatment options and the ability to use less-invasive methods.⁷ Despite advances in

Abstract. Early detection of ovarian cancer could greatly increase the likelihood of successful treatment. However, present detection techniques are not very effective, and symptoms are more commonly seen in later stage disease. Amino acids, structural proteins, and enzymatic cofactors have endogenous optical properties influenced by precancerous changes and tumor growth. We present the technical details of an optical spectroscopy system used to quantify these properties. A fiber optic probe excites the surface epithelium (origin of 90% of cases) over 270 to 580 nm and collects fluorescence and reflectance at 300 to 800 nm with four or greater orders of magnitude instrument to background suppression. Up to four sites per ovary are investigated on patients giving consent to oophorectomy and the system's *in vivo* optical evaluation. Data acquisition is completed within 20 s per site. We illustrate design, selection, and development of the components used in the system. Concerns relating to clinical use, performance, calibration, and quality control are addressed. In the future, spectroscopic data will be compared with histological biopsies from the corresponding tissue sites. If proven effective, this technique can be useful in screening women at high risk of developing ovarian cancer to determine whether oophorectomy is necessary. © 2010 Society of Photo-Optical Instrumentation Engineers. [DOI: 10.1117/1.3503468]

Keywords: endoscopy; tissue fluorescence; ovarian cancer; tissue spectroscopy; UVC excitation; fiber optic probe.

Paper 10249RR received May 9, 2010; revised manuscript received Aug. 31, 2010; accepted for publication Aug. 31, 2010; published online Oct. 27, 2010.

conservative treatment methods both invasive and noninvasive, screening for early detection of ovarian cancer is not yet available.⁸

Evaluation of the family history of breast and ovarian cancer along with genetic testing can identify women at increased risk of developing ovarian cancer. These women may benefit from additional diagnostic techniques to determine the optimal time of oophorectomy. Techniques allowing surveillance of the ovary have the potential to prolong fertility and will delay the morbidity associated with early onset of menopause. Furthermore, should proteomics testing⁹ be able to identify patients developing ovarian cancer, optical evaluation of the ovary may become the procedure of choice to perform a second diagnostic evaluation to minimize false positive results.

Several groups are investigating optical technologies to nondestructively image tissue at high resolution for the early diagnosis of ovarian cancer. Some of the promising methods are confocal microscopy,^{7,10-13} nonlinear microscopy,¹³⁻¹⁷ spectroscopy,¹⁴⁻¹⁷ and optical coherence tomography (OCT).¹⁸⁻²⁰

Optical spectroscopy could be used as a screening or diagnostic aid in the early detection of ovarian cancer. Amino

Address all correspondence to: Urs Utzinger, University of Arizona, Biomedical Engineering Department, 1127 East James E. Rogers Way, Tucson, Arizona 85721. Tel: 520-626-9281; Fax: 520-626-9287; E-mail: utzinger@u.arizona.edu

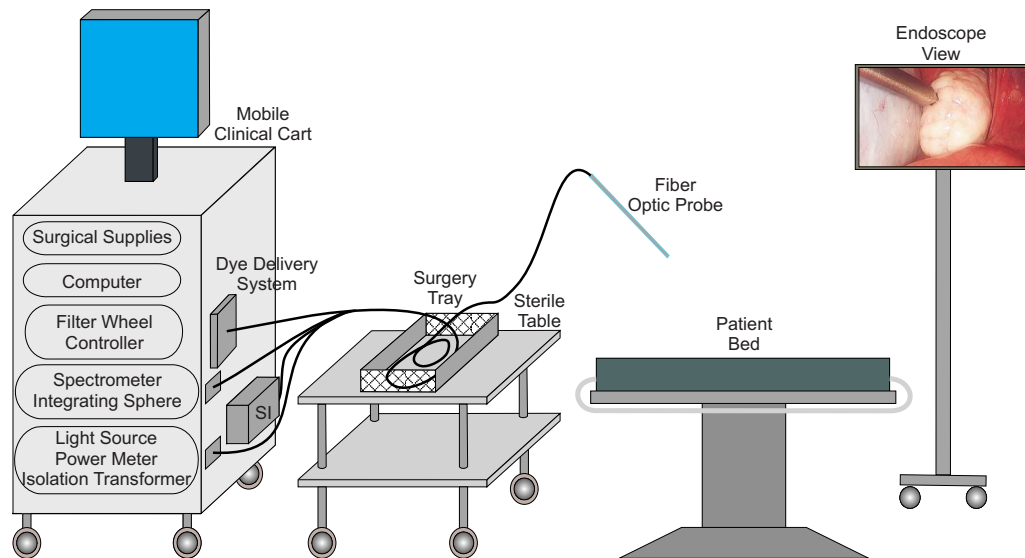


Fig. 1 Schematic of the CRD in a clinical setup. The CRD is to the left, followed by a sterile table on which a surgery tray containing the fiber optic probe is placed. The patient bed is to the right. The gross anatomy seen through a laparoscope is visible on the screen with the fiber optic probe in contact with the ovary.

acids (for instance, tyrosine and tryptophan), structural proteins (such as collagen and elastin), and enzymatic cofactors (for example, NADH²¹ and FAD) have fluorescence properties.^{22,23} Tyrosine and tryptophan are both excited near 280 nm, while tryptophan fluorescence dominates at 340-nm emission in tissue. NADH is highly fluorescent, with excitation and emission maxima at 340 nm and 460 nm, respectively. The oxidized form of NADH, NAD⁺, is minimally fluorescent. FAD can be excited around 450 nm and emits around 520 nm. In contrast to NADH, the oxidized forms of flavins are maximally fluorescent. Collagen and elastin when excited below 340 nm have emissions near 380 nm. However, different emission spectra are observed with longer excitation wavelengths and indicate a complex combination of fluorophores within collagen.^{24,25} The response of these biomarkers is a function of cell activity (proliferation, tumor formation, and so on) and composition of extracellular matrix.²⁶ Fluorescence can investigate changes in epithelial cell metabolism by assessing mitochondrial fluorophores such as the metabolic cofactors NADH and FAD. Epithelial–stromal interactions modify collagen cross-linking of the extracellular matrix, which can result in changes in fluorescence of these cross links.¹

The clinical research device (CRD) described here accesses the surface epithelium of the ovary with a fiber optic probe employed through an access port used for laparoscopy. The epithelial surface is excited over 270 to 580 nm, and emission is collected at 300 to 800 nm to best sample fluorophores present in the tissue. Currently, the CRD is being evaluated in a clinical trial at the University Medical Center (UMC), University of Arizona, with 40 patients with scheduled oophorectomy, to collect spectroscopic data (IRB Federal Wide Assurance Compliance: FWA00004218, Project No. 02-0495-01). The risk status of the study was evaluated by the data and safety monitoring board (DSMB) of the Arizona Cancer Center as well as University of Arizona's Institutional

Review Board (IRB) and noted as a nonsignificant-risk or low-risk study.

We describe the design and the selection of the components used in the CRD. The evolution of the fiber optic probe that is used to interrogate the ovary is discussed, and results on performance, calibration, quality control, and clinical use are presented. We compare the device with an industry-standard spectrofluorometer (Fluorolog, Horiba Instruments, Inc., Irvine, California) and demonstrate calibrated measurements on ovarian tissue during surgery.

2 Materials and Methods

The CRD is a comprehensive optical spectroscopy system and self-contained unit that can be used in a standard operating room (OR) to perform spectroscopic measurements on ovarian tissue *in vivo*. Each clinical measurement consists of accessing and exciting the ovarian surface epithelium through a laparoscopic access port (trocar) via a fiber optic probe. Collected light is spectroscopically analyzed and recorded for each measurement site. The setup of the CRD in the OR is shown in Fig. 1. An operator interfaces with the mobile clinical cart, while the fiber optic probe is set by the surgical staff on a sterile tray. The end of the probe with connectors to the light and data ports is connected to the CRD by the operator. The sterile part is picked up by the physician when the ovary is located and accessible for measurements. The measurement is conducted under endoscopic surveillance. A standard cart rack cabinet (E30-2002, Bud Industries, Inc., Willoughby, Ohio) houses all the components. Casters with locks and 4-in rubber wheels allow the system to clear small bumps common in hospitals and research laboratories (Luna Caster and Truck, Phoenix, Arizona).

A research protocol was developed with the gynecologic oncologists, allowing *in vivo* optical evaluation of the ovaries of patients undergoing planned oophorectomy. A health ques-

tionnaire is completed by the patient with the help of a research nurse, which is later used to evaluate the patient's risk status for developing ovarian cancer. Since the prevalence of ovarian cancer is relatively low, patients at moderate to high risk for developing ovarian cancer are given highest recruitment preference, as they have a higher probability of harboring premalignant changes in their ovaries.

The research protocol allows evaluation of up to four sites per ovary and collection of biopsies for histological purposes. An oophorectomy carried out in the UMC can be either a laparoscope-assisted or an open procedure. To perform an optical measurement, the surgeon first needs to locate the ovary in the peritoneal cavity. Connective tissue is removed if necessary without cutting the blood supply to the ovary. For a laparoscope-assisted case, the surgeon accesses the ovary through a 5-mm trocar. Once a site is selected and the probe is placed in contact with the ovary, the endoscope light is turned off and is replaced by illumination light from our fiber optic probe, which we can control with our instrument. In the case of an open surgery, overhead lights of the operating table and room lights are turned to minimal intensity throughout the duration of spectroscopic measurements. The remaining background light collected by our instrument is recorded and subtracted from the tissue recordings during post-processing. All the measurements are performed before the blood supply to the ovaries is transected. Selection of the measurement sites is based on the surgeon's expertise in identifying suspicious areas and in general includes two sites each on the anterior and posterior sides of the ovary. Suspicious areas on the surface of the ovary include cyst walls, nodules, abnormal masses, discolorations, and so on. Each site is annotated prior to removal of the ovary from the peritoneal cavity to aid biopsy retrieval, which because of the firm morphology of the ovarian surface, cannot be performed intraoperatively. Based on observation of the endoscope's video monitor, a drawing is sketched to illustrate the location of the measurement. To minimize risks from the measurement procedure, only ovaries planned for subsequent surgical removal are measured. Apart from the time needed to perform the optical measurements, there is no modification to the surgical procedure.

There were many practical challenges in the design, development, and maintenance of the CRD. First, for the excitation configuration, the tissue's UV light exposure needed to remain below the assumed threshold limiting value (TLV) deduced from comparable organ sites.²⁷ Furthermore, the out-of-band (OOB) light has to be suppressed with four or greater orders of magnitude ($\geq OD4$) to excite the fluorophores so that light reflected from the tissue will not appear as endogenous fluorescence.

Second, for the emission detection configuration, the optical signals returning from the measurement site are weak, requiring suppression of the system's autosignals (e.g., fluorescence originating in the optical components of the CRD). Fluorescence collected from epithelial tissues with fiber optic probes is in the range of 0.01 to 0.4% of the excitation light.²⁸ If excitation light is scattered in the spectrometer, it will be misinterpreted as fluorescence, so we require that the reflected light be suppressed at OD4 or better. The detected signal-to-noise ratio (SNR) needs to be 200 or better for quality control.

Third, for clinical operation, the electrical safety of the CRD had to be within the hospital's clinical engineering re-

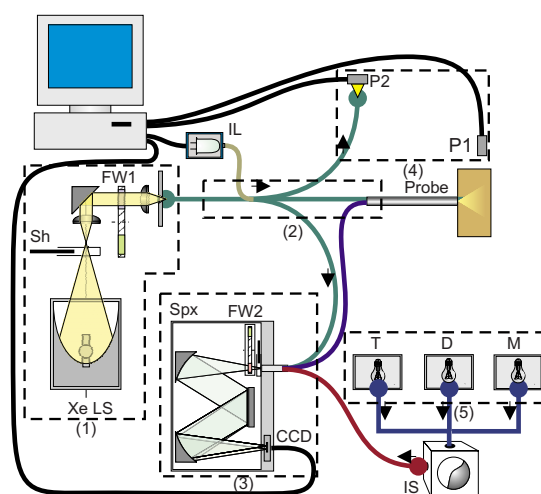


Fig. 2 Illustration of the optical spectroscopy system used in the CRD. It consists of four main components: (1) an excitation light source comprising an arc lamp combined with filter wheels and a fiber optic coupling system, (2) a fiber optic probe that directs light onto the tissue and collects fluorescence and reflected light, (3) a spectrograph that includes a thermoelectrically cooled CCD, (4) and (5) calibration components. Sh and FW1 represent the light source shutter and light source filter wheel. SI is the surgical illuminator, while P1 and P2 are the two configurations of the power meter. T, D, and M represent tungsten-halogen, deuterium, and mercury calibration light sources. IS is an integrating sphere providing uniform illumination of the fiber optic probe during calibration measurements. Spx represents a spectrometer, while FW2 and CCD represent the filter wheel and camera in the spectrometer.

quirements. Space limitation in the OR requires the instrument to be packaged into a mobile cart. Clinical measurements must be completed within the time frame approved by the IRB.

Fourth, the fiber optic probe developed has to be ergonomic and sterilizable. The ergonomics of the probe is important so that the physician can hold the probe in contact with the surface of the ovary for the duration of a clinical measurement. Sterility of the probe is required to use it intraoperatively. Fifth, and one of the biggest challenges, was marking the area of the biopsy so that the spectroscopic data accurately reflected the histology.

Last, the recorded data needed to be calibrated and quality controlled to free it from random and systematic errors, to exclude device failure and ensure repeatable performance throughout the duration of the study.

The schematic of the spectroscopy system showing the different components that are integrated to form the functional units of the CRD is shown in Fig. 2. The excitation light is routed to the tissue or sample of interest using a fiber optic probe, and the fluorescence and reflectance emitted are carried back by the probe to be analyzed. The data acquisition process is fully automated and computer controlled.

2.1 Excitation Light Source

The excitation light source is a critical part of the CRD, as it provides the tissue-exciting light and needs to be optimized for low OOB light in the UV and visible. It is based on a custom light source using a 75-W Xenon short arc lamp [UX-

75XE, Photon Technology International (PTI, Birmingham, New Jersey] in a lamp housing (A1010B and LPS-220B, PTI) with an $f/2.5$ elliptical reflector creating a spot size of 3.2 mm (FWHM). This results in a high power density at the focus, which is ideal for coupling light into a small fiber bundle. An integrated igniter (LPS-221B, PTI) provides the required high preignition voltage to start the lamp and interferes minimally with other electronic equipment. A shutter with a 6-mm aperture and blades coated with AlMgF_2 (VS2581ZMO, Vincent Associates, Rochester, New York) controls light exposure that is synchronized with the camera electronics. A plano-convex quartz lens ($f=50$ mm) is used for collimating the light beam through a 10-position filter wheel (Lambda 10, Sutter, Inc., Novato, California) carrying 10 filters (Semrock, Rochester, New York, Chroma Technologies, Rockingham, Vermont, and Omega Optical, Brattleboro, Vermont) with low autofluorescence (AF) and high OOB suppression. One filter is a long-pass filter with a cut-on at 320 nm for reflectance measurements, and the other nine filters were bandpass filters used to excite fluorescence. Their center wavelengths (λ_{center}) were selected to excite endogenous fluorophores mentioned earlier that have the potential to serve as biomarkers. A second lens similar to the first is used to focus the light beam into the fiber bundle. The lenses were chosen (infinite conjugates) to match the NA (0.22 in-air) of the fiber bundle. A pinhole aperture is placed in the beam path to block stray light. The light source assembly is cooled by an external low-noise fan (624N, ebmpapst, Inc., Mulfingen, Germany).

2.2 Spectrometric Detection

Detection of fluorescence and reflectance signals is carried out using a diffraction-grating-based spectrometer (Inspectum 300, Acton Research Corporation, Acton, Massachusetts). This spectrometer uses a Czerny-Turner optical configuration, which provides better stray light suppression than other compact spectrometers that are based on single mirror devices. It also has a built-in filter wheel, which is necessary to suppress excitation light reflected into the spectrometer. The mirrors are corrected for astigmatism, allowing multiple independent spectra to be collected independently. The spectrometer has an integrated back-illuminated CCD (INS-122B, Hamamatsu, 1024×122 pixels, $24.6 \text{ mm} \times 3 \text{ mm}$) that is cooled to -20°C to lower the dark current when exposure reaches multiple seconds. Back-illumination provides higher quantum efficiency ($\eta \sim 85\%$) than a comparable UV-coated front-illuminated CCD. The spectrometer has an internal shutter and mechanism to adjust the input slit size. The optical fibers themselves form a $200\text{-}\mu\text{m}$ limiting aperture at the slit. A single 150 grooves/mm grating (1-015-300, Newport Corporation, Irvine, California) was set to a center wavelength (λ_{center}) of 546 nm to match the spectral range of interest and to match the peak wavelength of the mercury spectrum (546.1 nm). The grating was optimized for the UV-blue (η at $300 \text{ nm}=73\%$) to minimize the exposure when the sample is illuminated with short wavelengths.

For fluorescence measurements, excitation light can be reflected into the detection channels and should therefore be well-suppressed. This is achieved by placing a rotating five-position filter wheel in the CCD's field of view. Five long-pass filters were selected to provide the suppression needed

for the excitation light. Due to the limited number of filter positions (total of 5 positions), one long-pass filter position had to suppress more than one excitation wavelength (total of 10 positions). These filters are dielectric coated and thus have minimal AF, and also they are placed away from the conjugate plane of the CCD.

For reflection measurement, the detection spectrum has second-order light, as the spectrometer used is a grating-based device. Thus, two reflection measurements are carried out, one with the shortest long-pass filter and the other with long-pass filter at around 400 nm.

2.3 Fiber Optic Probe

The fiber optic probe is designed to transport the excitation light to the ovarian surface and carry back the emission and reflectance for spectrometric detection.²⁹ Through the duration of this project, three generations of fiber optic probes were developed. The differences in the three generations of the probe are summarized in Table 1. Their development was based on feedback from the physician and also practical limitations observed while using them to perform clinical measurements. The excitation and emission collection elements are identical in all three versions, and they primarily differ in their ergonomics and support of biopsy collection. Carbon dioxide insufflated peritoneal pressure³⁰ is maintained in all three versions. We tested each of the three generations of fiber optic probes in a laparoscopy simulating training module (Karl Storz GmbH & Co., Tuttlingen, Germany). For this purpose, a phantom based on porcine collagen was used to simulate the surface toughness and texture of an ovary.

For biopsy collection of the probed sites, we attempted *in situ* biopsy; however, standard retrieval with forceps is not feasible, and biopsy with surgical blades imposes additional risks to the patient. Thus, annotation of these sites is important for biopsy retrieval once the ovary is excised from the body. This is addressed by using a 20-gauge needle (0.032-in OD, 0.020-in ID, HTX-21R, Small Parts) custom-made (Vita Needle Company, Inc., Needham, Massachusetts) through a syringe channel in the probe. A few μL of sterile tissue-staining-dye (methylene blue) is used at its tip.³¹ A pump (NE-1000, New Era Pump Systems, Inc., Wantagh, New York) is used for dispensing the dye using a 12-ft medical-grade tubing (US Plastics, Lima, Ohio). The needle is introduced into the fiber optic probe by the OR technician before the probe is inserted into the trocar. A spring (CSXX-0080, Small Parts) prevents the syringe from protruding out of the fiber optic probe. Often, the indentation of the syringe is sufficient to identify the measurement locations. Synchronized illumination of the field of view was incorporated, as the endoscope illumination must be turned off during measurements (as to not interfere with tissue emission collection). The probe tip uses one inch of transparent medical-grade polycarbonate (Zelux GS, Westlake Plastics, Lenni, Pennsylvania), and the surface is rough-polished with a grit size of 220. Illumination light is coupled into its proximal end, and when it reaches the rough surface, it is scattered, which illuminates a larger field compared to the previous probes. This allows the probe to be held steady when the endoscope illumination is turned off. In addition, at 120 lumens, the white-light LED (LXK2-PW14-V00, Philips Lumileds Lighting Co., San Jose, California) is

Table 1 Comparative summary of fiber optic probe features over its three generations.

Features	First generation	Second generation	Third generation
Patient cable length	3 m	4 m	4 m
Surgeon illuminator	No	Yes	Yes
Dye marking capability	No	Yes	Yes
Illumination type	NA	Fiber illumination	Diffuse illumination
Illumination LED	NA	45 lumens	120 lumens
Illumination efficiency	NA	Lower	Higher
Laparoscope compatibility	External adaptor	Integrated	Integrated
Probe length (inches)	20	20	14
Laparoscopic pressure	MGES ^a O-ring	Trocar	Trocar
Maintenance			

^aMedical grade and ethylene oxide sterilizable.

three times brighter than that of the first-/second-generation probes.

The packaging of the third-generation probe and the layout of the optical fibers representing its different functioning legs are illustrated in Figs. 3(a) and 3(b). This figure shows the configuration of the fibers used for excitation, illumination, emission, calibration, and quality control. Four fibers route the excitation light to the tissue, and the tissue emission is collected by three fibers that route it to the spectrometer. These seven fibers (200 μm , Polymicro) are interfaced to a short single central fiber (CF) (800 μm), allowing homogeneous illumination over an 800- μm area at the probe tip. Light from the light source is directly coupled with a fiber (200 μm) for power measurements. A feedback fiber (70 μm) couples light from the light source directly into the spectrometer to monitor bandpass filter failures. A fiber (200 μm) carries light from an integrating sphere to the spectrometer and could be used for calibration purposes. NA (in air) of all the fibers employed is 0.22. There are 21 illumination fibers that provide auxiliary illumination for visual feedback, and these fibers terminate into the polycarbonate tip of the probe, providing illumination of the surgical field. The length of the probe was chosen to be comparable to an OR suction irrigator, which is 14 in in length and fits down a standard 5-mm trocar. A stainless steel hypodermic tube (OD 4.77 mm, HTX 06-1/2R, Small Parts) defines the length and diameter of the rigid part. The optical sampling fibers are housed in a smaller tube (OD 1.27 mm, HTX-18T, Small Parts) and stick out about 0.5 mm at the probe tip. Between the rigid probe and the instrument, braided stainless steel monocoil with PVC (Armor Associates, Inc., Malvern, Pennsylvania) is used for protection of the fibers.

The fiber optic probe consists of several materials. The components that come in direct contact with the patient and physician are made of medical-grade materials such as stainless steel assembled using medical-grade epoxy. Chemically inert materials were used at all other assembly locations of the

probe. Two assembly locations are of particular interest with respect to the type of glue employed: the junction connecting the excitation–emission fibers to the single fiber used for light mixing, and the probe tip where excitation light can be scattered by the sample and epoxy. These areas could fluoresce and add to the measurement signal. To reduce this, care was taken during fiber optic probe assembly to keep those areas glue-free. To minimize AF of the epoxy used, several industry-standard medical-grade epoxies were tested for their AF to determine the one that could be used for probe assembly. Measurements were performed on glue samples embedded in identically sized hypodermic needles, and the fiber optic probe was placed in direct contact with the glue samples. Measurements were performed on the Fluorolog using the fiber optic probe. The excitation and emission configurations covered the spectral region used for patient measurement. Furthermore, the excitation and emission fibers used have a high-OH fused silica core to allow ultraviolet C light transmission and have an aluminum jacket to keep their AF low in the presence of excitation light.

After each clinical use, the fiber optic probe and the dye delivery tubing are rinsed with Medical Enzyme detergent (Enzyme Solutions, Inc., Garrett, Indiana), cleaned with ethanol and cold sterilized using 100% ethylene oxide (EtO) at 90 to 135F using a dual cycle Steri-Vac 5XL gas sterilizer and aerator (3M, St. Paul, Minnesota).

2.4 Calibration

Calibration of the data is important to factor out device-related parameters and was divided into power, spectral, and wavelength calibrations. Power calibration ensures that power incident on the tissue is always recorded. It is performed by taking a ratio of power at the probe tip and at the termination of a fiber directly coupled to the light source, each by using a power meter (1830-C, Newport) with a UV-enhanced silicon-based power meter sensor (883-UV, Newport).

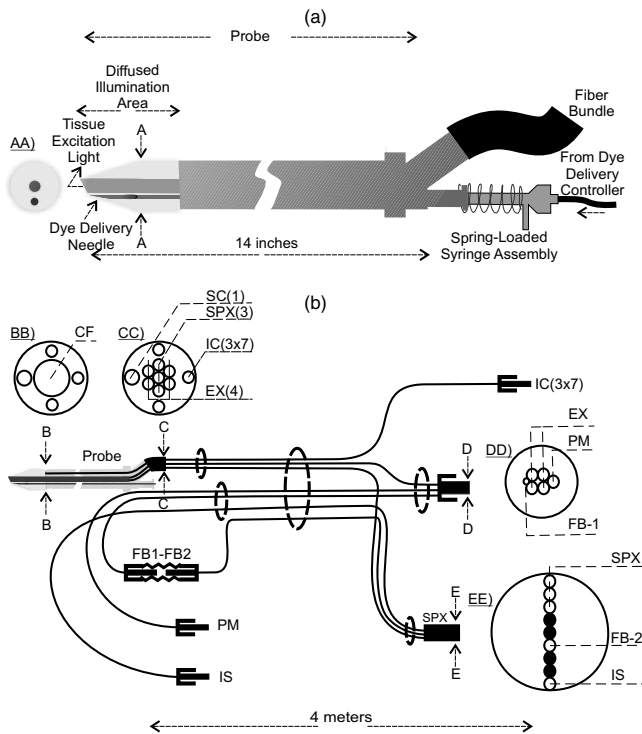


Fig. 3 (a) Packaging of the third-generation fiber optic probe. Section AA shows the cross section of the probe tip where the excitation light, diffused illumination light, and spring-loaded syringe emerge. (b) Illustration of the optical wiring diagram. EX and SPX are the excitation and emission fibers interfacing with CF, the central 800- μm fiber. IC represents the 21 illumination channel fibers. Section BB presents the cross section of the probe where the IC fibers (3 \times 7) terminate and the syringe channel (SC) goes through. Section CC illustrates the seven EX-SPX fibers, the 21 IC fibers and the through syringe channel. PM, FB-1, 2, and IS are the power meter, feedback, and integration sphere fibers, respectively. The EX, PM, and FB-1 fibers are bundled together and terminated with a FC connector (section DD). They are simultaneously illuminated by the light source. IS is the integrating sphere fiber. The interface FB-1-FB-2 is for monitoring bandpass filter failures. The SPX, FB-2, and IS fibers are bundled together and terminated in a linear arrangement with a ferrule that fits the entrance slit of the spectrometer (section EE).

Spectral calibration ensures that the emission is collected independent of the sensitivity fluctuations over the spectral range of interest. Deuterium and tungsten-halogen light (DH2000, Ocean Optics, Dunedin, Florida) sources cover the spectral range of interest, and their output is measured at each emission filter configuration and compared with the manufacturer's data to generate a sensitivity calibration curve. The spectral calibration ranges are 200 to 400 nm and 380 to 800 nm, respectively, with a spectral overlap from 380 to 400 nm.

Peaks of a mercury-argon calibration source (HG-1, Ocean Optics) are used to convert the linear array of pixels needed to wavelength-calibrate the spectrometer. Because the spectrometer rotates the grating turret during each power-up, this calibration is performed as part of each calibration sequence.

2.5 Data Processing

When analyzing the light path from source to sample to detector, one can identify the transfer functions involved. The

light source is subjected to an excitation power transfer function prior to exciting the sample, which is determined by the throughputs of the filters and the fiber optic probe. Based on its composition, the sample converts the excitation light to fluorescence, and the amount collected also depends on the probe geometry. We did not further consider those, as they were kept constant by establishing probe-tissue physical contact. The fluorescence emitted is subjected to a detection transfer function based on spectral transmission of the fiber optic probe, emission filters, wavelength-dependent efficiency of the grating, and the detector's spectral sensitivity. Integrating over the excitation bandwidth, one can show that the recorded fluorescence is proportional to the parameters described in the equation:

$$F_{\lambda_{ex}\lambda_{em}} = \frac{F_{rec}[J]}{A[\text{cm}^2] \cdot \Delta t[\text{s}] \cdot I_{\lambda_{ex}} \left[\frac{\text{W}}{\text{cm}^2} \right] \cdot P_{\lambda_{ex}} \cdot \eta_{\lambda_{em}}}, \quad (1)$$

where $F_{\lambda_{ex}\lambda_{em}}$ is the fluorescence from the sample measured at λ_{ex} and λ_{em} , F_{rec} is the recorded fluorescence, A is the exposed area, Δt is the exposure time, $I_{\lambda_{ex}}$ is the excitation power at λ_{ex} , $P_{\lambda_{ex}}$ is the excitation power transfer function at λ_{ex} , and $\eta_{\lambda_{em}}$ is the emission-collection efficiency transfer function.

The recorded fluorescence is the intensity values on the CCD detector. The exposed area is kept constant in our study, and the exposure time is set by the control software. It is kept constant for all excitation wavelengths but is changed when measuring calibration standards. The excitation power is obtained by power calibration. The emission-collection efficiency transfer function is determined based on the spectral calibration.

In order to produce calibrated fluorescence spectra, the process described in Fig. 4 is employed. Spectrally dispersed light is recorded on the spectrometer output plane. For each measurement, an image is recorded with the light source shutter closed. The subtraction of those two images will eliminate room light and dark current of the sensor. The vertical direction of the image encodes for fiber location on the spectrometer input slit. Data along that direction are summed to create a single spectrum. The horizontal direction of the image encodes for wavelength, and based on the wavelength calibration, we convert pixel location to wavelength. Since the detector oversamples the spectrum, noise removal with a Savitsky-Golay³² filter was employed to match the systems optical resolution. By the multiplication of the computed power calibration factor of the excitation light and correcting by the spectral sensitivity of the detector, we can compute a calibrated fluorescence spectrum. Assembling all the emission spectra into a matrix yields an excitation emission matrix (EEM).

2.6 Quality Control

In addition to calibration, it is important to develop a quality control protocol to ensure repeatable performance of the CRD throughout its lifetime. The spectral output and power of the light source at each excitation filter configuration are measured. The feedback fiber illustrated in Fig. 3(b) is used for monitoring any bandpass filter leaks. The passbands of those

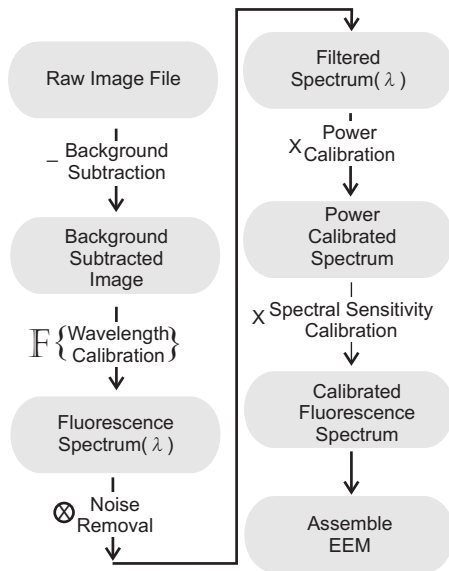


Fig. 4 Flowchart showing the CRD data processing sequence. Raw images from the spectrometer camera and background data (excitation shutter closed) were acquired for every site during patient measurements. Wavelength calibration transformed the background-subtracted data from pixel-space to wavelength-space. Noise removal was performed using Savitsky-Golay filtering (order=2, window size = 15) (Ref. 32) to match the system's resolution. The filtered spectrum was calibrated by the excitation power and the spectral sensitivity of the device. Several spectra were finally assembled to an excitation-emission matrix (EEM).

filters can be monitored by coupling light from the fiber optic probe to the input port of an integrating sphere (IS) and monitoring its output port with an IS fiber [Fig. 2 and Fig. 3(b)]. Positive and negative fluorescence and reflectance standards that cover the spectral range of interest were included in the measurement procedure. These standards had peaks at excitation and emission wavelengths throughout the spectral range of the CRD. The positive standards include p-Terphenyl, Tetraphenylbutadiene, Rhodamine, and Fluorescein (Starna Cells, Atascadero, California). The first three standards are fluorescence standards dissolved in methylmethacrylate and polymerized to produce a polymethyl methacrylate (PMMA), while Fluorescein is a liquid fluorescence standard in a quartz cuvette. The negative fluorescence standard is deionized (DI) water in a dark bottle, which has a very low AF. For reflectance measurements, the positive standards are microspheres dispersed in DI-UV water in a 1-cm path length quartz cuvette and an integrating sphere coated with broadband reflecting Spectralon³³ of 2-in inner diameter.

In order to calculate the signal-to-noise ratio of the measured signals, we filtered the raw data with a Savitsky-Golay filtering (order=2, window size=15 pixels). This processing resulted in a filtered spectrum that has the same number of elements as the raw spectrum but matches the spectrometer's resolution. The noise spectrum was then obtained by subtracting the original spectrum from the filtered spectrum. A single number describing the noise was determined by calculating the standard deviation over a window of 150 pixels (75 nm) located at the maximum of the fluorescence spectrum. This number describes the noise of the raw spectrum. As the filter

processes occurred over a window size of fifteen pixels, one can estimate the noise remaining in the filtered spectrum to be a square-root of 15 smaller. SNR is the peak intensity of the fluorescence signal divided by the standard deviation of the noise.

The calibration and quality control measurements are performed within the OR using a dark box to baffle room light. LabView (National Instruments, Austin, Texas) software is used to automate all the measurement procedures and for data storage. The drivers developed for the shutters, filter wheel, power meter, camera, and spectrometer are interfaced by custom-written LabView programs (RCubed, LLC, Lawrenceville, New Jersey). A script engine is used to select scripts that automate patient measurements, calibration, and quality control routines, and a separate batch file is generated to plot the data.

3 Results

3.1 Excitation Light Source

The design goal of the light source was to achieve an OOB suppression of four orders or better at wavelengths where fluorescence occurs. Several bandpass filters from three different manufacturers (Semrock, Chroma, and Omega) were investigated, and we found that it was more difficult to achieve the design goal with filters below 400 nm. The output of the configuration was analyzed by the Fluorolog. Figure 5 illustrates the best and worst cases of our configuration. Several filters did not operate at the desired specifications, and the suppression levels were improved by placing two filters in series, resulting in the desired OOB level. Table 2 illustrates the filter configuration that we implemented in our system and lists the combination of the excitation filter with corresponding emission long-pass filter in the spectrometer, which is needed to suppress the reflected excitation light. We chose long-pass filters with dielectric coatings with OD 5 or better OOB suppression and having cut-on wavelengths at 300, 372, 420 (Chroma), 500, and 590 nm (Omega). Excitation light used for reflectance measurement passes a 320-nm longpass filter and is additionally attenuated by three orders of magnitude to avoid detector saturation. The total UV tissue exposure was calculated using a technique published by ACGIH wherein its threshold limiting value (TLV) was computed based on the effective irradiance relative to a monochromatic source at 270 nm. The exposure was determined to be less than 12% of the TLV set for UV exposure when light exposure is 0.2 s at each excitation wavelength. Of the 12%, 11 is from exposure at 280 nm (Table 2). Reflectance is collected by overlapping (300 to 600) and (420 to 800 nm) with two measurements to achieve data from 300 to 800 nm.

3.2 Spectrometric Detection

The image plane of the detector contains three individual spectral tracks, with the largest track occupying the light collected from the sample and two additional tracks allowing feedback and quality control measurements of the instrument. Our fiber arrangement at the input slit of the spectrometer resulted in minimal cross talk between the tracks measuring sample spectra and that conducting instrument quality control.

The camera driver allowed binning of the data in spectral (horizontal) and measurement track (vertical) direction. Since

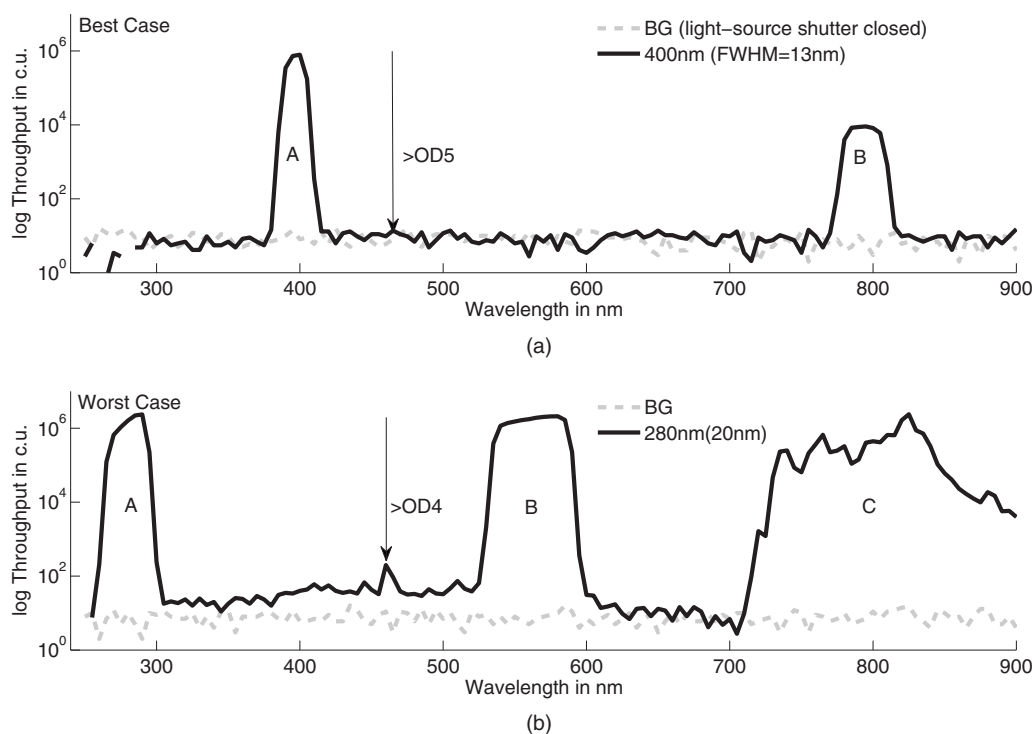


Fig. 5 (a) Best and (b) worst cases of out-of-band suppression of the excitation light source measured for 400-nm and 280-nm excitation filters, respectively. A and B in both graphs represent the pass-band for the excitation configuration and its second order. The regions between them, in both cases, represent the out-of-band region where fluorescence is measured. C represents the light leaking through the filter in the infrared. The out-of-band light intensity in (a) is on average 5 orders lower than the pass-band, while in (b), it varies from 4.1 to 4.9 orders. The remaining excitation configurations have an out-of-band suppression of OD 4.8 or better.

Table 2 Filters employed in the CRD.

Measurement type	Excitation filter λ_{center} (nm) BW (nm)	Emission filter cut-on (nm)	Effective transmission (%)	Power delivered (μ W)	TLV Safety (%)
Fluorescence	280 ^a (20)	300	57	9	11.10
	320 ^a (17)	372	60	50	0.18
	340 ^a (34)	372	55	63	0.03
	370 ^a (20)	420	90	34	<0.01
	400 ^b (13)	420	40	36	<0.01
	415 (30)	500	70	205	<0.01
	440 (21)	500	60	128	NA
	480 (23)	500	80	224	NA
	555 (30)	590	80	348	NA
Reflectance	Cut-on at 320 and OD3	300, 420	0.093	45	0.6

^aTwo identical filters in series.

^b400-nm bandpass filter followed by a short-pass filter to suppress out-of-band light.

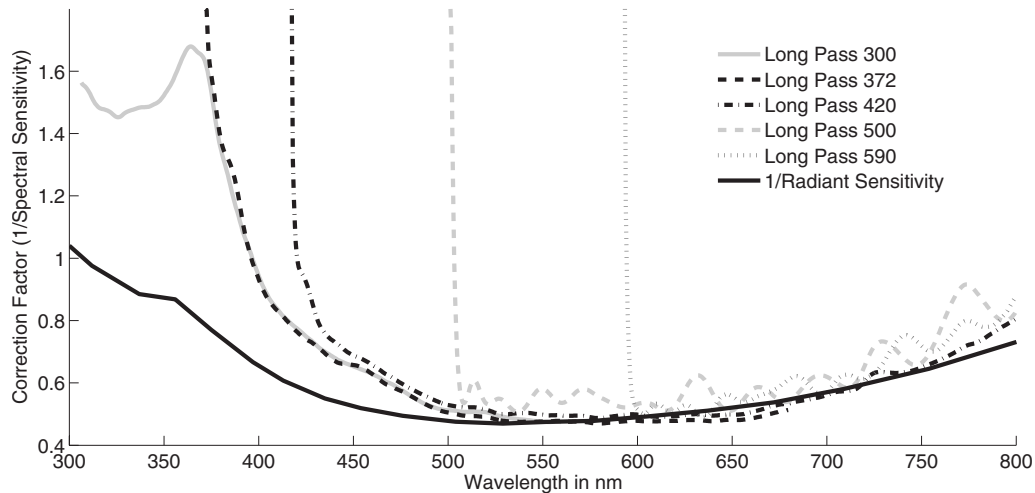


Fig. 6 The CRD spectral-sensitivities for the five different long-pass filter configurations (300, 372, 420, 500, and 590). The first three filters (Chroma Technology) have smoother responses in comparison to the last two filters (Omega Filters). In addition, the curve composed of the device's CCD quantum efficiency and the spectrometer's grating efficiency is plotted and shows relative good agreement in the visible. The detection sensitivity is highest in the visible and is lower in the UV and near-infrared. The detector and spectrometer have been optimized for UV sensitivity.

binning occurs on the detector, it reduces readout noise and the amount of data that needs to be read out and transferred. Binning was optimized to not saturate the readout register and to not compromise system resolution while minimizing time needed to readout the data. In the vertical, a pixel-binning of eight was achieved and increased read-out speed by 55% when compared to unbinned readout. Binning in the horizontal direction did not improve read-out speed, indicating that the detector does not include electronic hardware for this operation. Binning is not appropriate for high signal levels such as some of our calibration standards, because it would saturate the readout register. Signal intensity can be decreased by reducing the exposure time; however, the camera drivers take significantly longer to reprogram the exposure time as compared to the binning. Therefore, the exposure time was optimized for the low light levels, and binning is disabled for high-light-level signals.

Correction factors due to wavelength-dependent sensitivity of the instrument are illustrated in Fig. 6 for measurement configurations. Fluctuations in the pass band and steep cut-on characteristics are typical for dielectric coated long-pass filters. An approximation of the system's spectral sensitivity without long-pass filters is represented with the radiant sensitivity curve, which is directly proportional to the wavelength-dependent quantum efficiency of the detector and the grating efficiency. The spectral resolution of the detection system is determined by the size of the entrance slit image on the detector. In our case, the entrance aperture is a 200- μm -diam fiber. Given a pixel size of 24 μm , a grating with 150 grooves/mm and a focal length of 300 mm, the spectral resolution is 5 nm and 9 times oversampled.

3.3 Fiber Optic Probe

The fiber optic probe development primarily improved ergonomics, as the sample illumination and signal collection were not altered compared to previously employed fiber optic probes.²⁶ We were able to incorporate both site annotation as

well as visual illumination features. Annotation of the measurement site with the dye proved to be difficult, as delivery of precise dose depends on length of the tubing and hydrostatic configuration between annotation site and dye delivery pump. Also, excess dye blocked the tip of the probe. It turned out that a small needle puncture was sufficient to identify samples for later biopsy and processing, and inclusion of dye was abandoned. Using a 5 \times optical eyepiece along with an anatomical sketch of the measurement location on the ovary improved the probability of finding the punctured site. This technique is ineffective for cystic ovaries, as they are fluid filled and should not be punctured. In our experience, about half of the punctures could be located. In the case of sites that did not have an identifiable puncture, we consulted the anatomical sketch to estimate the most probable location for the biopsy matching the measurement site. This approach is relatively straightforward, as the measurement is taken and the location is noted in the context of the blood supply, the tube, and the attachment to the uterus. Even if a puncture mark is not seen, the location can be approximated in a reasonably accurate manner. The approximate imaging depth of our probe is 50 to 120 μm , assuming that glandular breast tissue³⁴ and ovary have similar optical properties and that the optical diffusion constant³⁵ approximates the average imaging depth.

We required the glue used to assemble the fiber optic probe to have lower AF in comparison to tissue fluorescence. To confirm this AF, four different types of glues were compared in fluorescence to average normal ovary using the Fluorolog (Fig. 7). The results showed that among the tested excitation wavelengths, 280 nm gave the strongest AF for all the glues and was nearly comparable to that of tissue fluorescence. Except below 320 nm, the AF from Ångström Bond 9320 is lower than tissue fluorescence and is the lowest among the other glues tested and so was selected as the glue of choice. The other components of the fiber optic probe that do not come in contact with the sample or the excitation light were assembled with glues that have high metal-metal shear

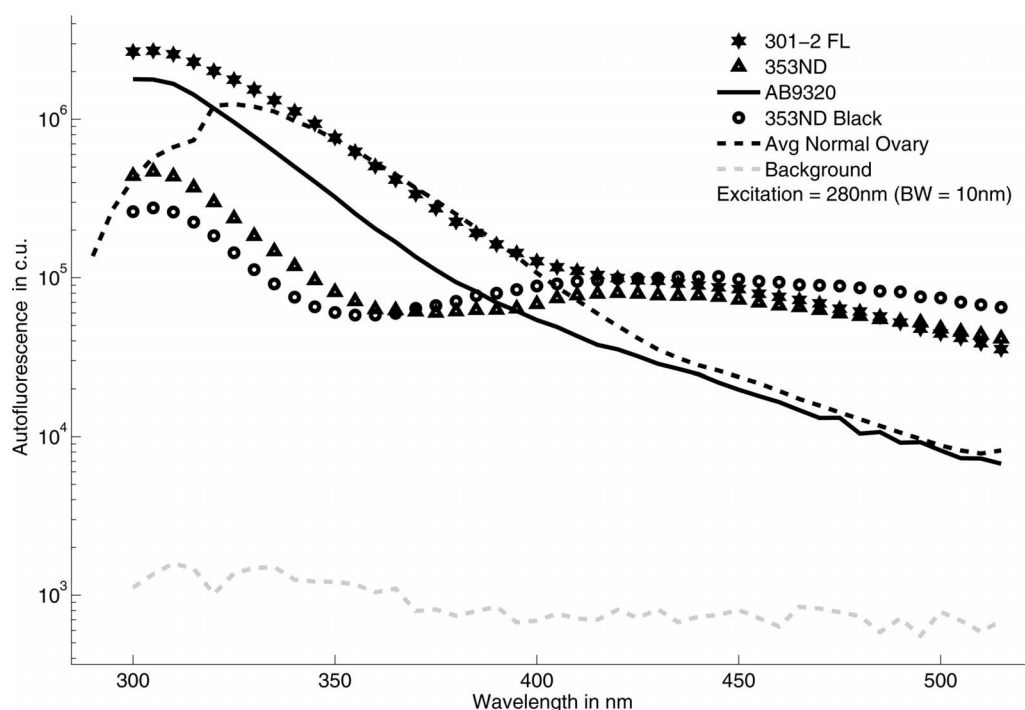


Fig. 7 Choice of glue employed in the fiber optic probe. Except below 320 nm, the AF from AB9320 is lower than tissue fluorescence and is the lowest among the other glues tested. 353ND black works better below 320 nm and has the lowest AF and is lower than tissue fluorescence by a factor of ~ 4.5 , while AB9320 is ~ 1.5 times higher. At all other excitation wavelengths, AB9320 exhibits the lowest AF.

strength and relatively low curing temperatures. Furthermore, multiple ETO sterilizations of the fiber optic probe and the dye tubing did not degrade them with time.

3.4 CRD Performance

To ensure electrical safety, a hospital-grade isolation transformer with a 1000-W capacity (ILC-1000MED4, Shoreview, Minnesota) was used to reduce the leakage current to less than $40 \mu\text{A}$, a tenth of the standard hospital electrical safety limit, while the ground continuity was less than $210 \text{ m}\Omega$, two-thirds of the maximum allowed. Thus, there was no electrical continuity to the fiber optic probe. The total power consumption of the CRD was measured to be about 750 W.

Since our protocol requires that measurements are completed within 10 min, we evaluated the timing efficiency of our instrument. With the latest firmware upgrades and the automated LabView programming sequences, each measurement sequence takes approximately 20 s (Table 3). The total sample exposure time was 4.4 s. We were able to start changing the excitation filters when camera data were transferred to the computer; however, this was not possible for the emission filter wheel.

The emission fibers carrying the fluorescence/reflectance signals operated at a working F/# of 2.27. Since the spectrometer used for detection of these signals operated at a system F/#=4 and 300-mm focal length, there is a loss of 60% of the detected emission signals.

Results from positive and negative standards with their respective comparison to the measurements on the Fluorolog are illustrated in Fig. 8. Emission and excitation spectra were

extracted from the respective EEMs. Good agreement was found for the systems, indicating that the calibration procedure for both excitation and emission-collection transfers were successful throughout the whole measurement wavelength range.

Because the power of our light source is decreasing with time, we monitor the power to determine optimal time of bulb replacement. There is a 3 to 8% power fluctuation per hour, while the fluctuations from one measurement day to the next one are 13 to 15%. This illustrates the importance to record power data for every CRD measurement. The power calibration factors (between power at probe tip and power at feed-

Table 3 Measurement timing efficiency for a single measurement.

LabView operation	Average time (ms)	Count	Total
Save data	20	22	440
Spectrometer filter change	1200	5	6000
Camera acquire (exposure time) ^a	540 (200)	22	11880
Shutter enable/close	30	44	1320
Total measurement per site is 19 to 20 s.			
Total camera exposure is ~ 4.4 s.			

^aLight source filters changed during data transfer.

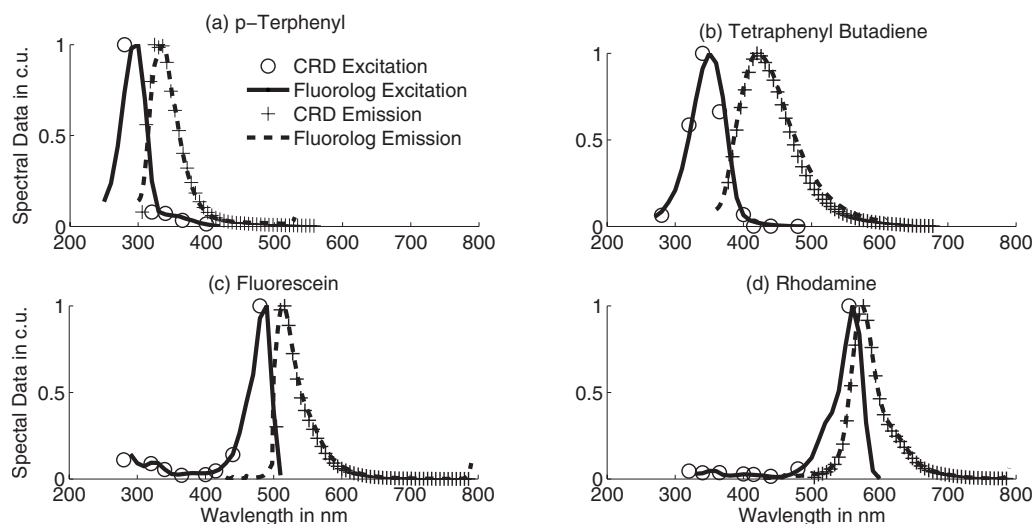


Fig. 8 The CRD measurement accuracy in comparison to measurements performed on the Fluorolog. The plots show the comparison of the excitation and emission spectra for the two devices using the same fiber optic probe. Measurements are performed on fluorescence standards. (a) through (d) show that the CRD measurement results (o, +) closely follow those from the Fluorolog. (a) Excitation range (EX)=270 to 290 nm, emission range (EM)=305 to 440 nm; (b) EX=310 to 355 nm, EM=390 to 510 nm; (c) EX=400 to 490 nm, EM=504 to 530; and (d) EX=400 to 450 nm, EM=596 to 620 nm.

back fiber) were at 3.7 ± 0.1 at all wavelengths except at 280 nm, where it was 3.2. As expected, the ratio is not varying much over the excitation range as the fiber throughput and chromatic aberrations of the coupling system did not appreciably vary.

SNR of ≥ 200 is accomplished for all measurements involving calibration standards without saturating the camera. Our ongoing clinical study indicates that all patient measurements have an SNR of larger than 110, which occurs at 555-nm excitation when using an exposure time of 0.2 s.

Results from a clinical measurement are presented in Fig. 9 from a normal ovary of a 62-year-old postmenopausal fe-

male. Emission spectra from the EEM are illustrated in the subplots and with the corresponding background measurement in water. In this example, measurements from the tissue are at least half an order larger than the background at all excitation wavelengths. Highest signal-to-background ratio was found at 320 nm and 340 nm, where AF from the tissue was high. AF of tissue at 280 nm is 2 times larger than in UV-A range, which is 12 times larger compared to the blue excitation range. A slight dip at 420 nm and ripples at 560 nm are due to hemoglobin reabsorption of the emission. In summary, the key CRD parameters and their values for the excitation and emission detection configurations, its clinical

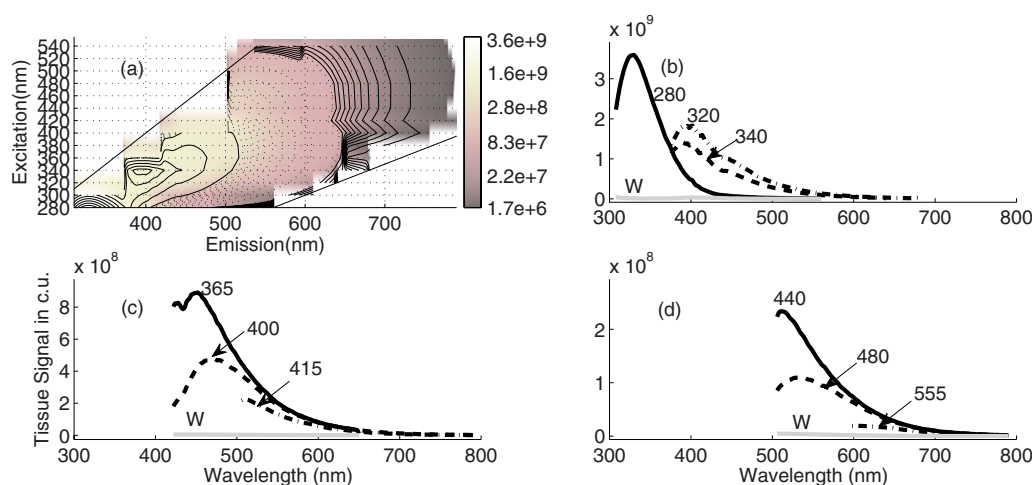


Fig. 9 Single calibrated and processed clinical data compared with its background (water). (a) Complete excitation–emission matrix (EEM) representing fluorescence intensity data at the measured site. The contours represent areas of equal intensity. (b) The emissions collected when the site is excited at 280, 320, and 340 are at two or more orders higher in magnitude than the corresponding background. (c) The ones at 365, 400, and 415 are an order or more higher, while (d) the ones at 440, 480, and 555 result in higher than half an order when compared to background. Fluorescence spectra are background-subtracted. Fluorescence in (b) is an order of magnitude larger than (c), which is approximately 5 times larger than (d).

Table 4 Performance summary of the CRD.

CRD parameter	Specification
Excitation configuration	
UV safety for tissue exposure at 270 nm	12% of threshold limiting value set by ACGIH
Excitation	270 to 580 nm
Excitation bandwidth	13 to 35 nm
Out-of-band suppression	\geq OD 4
Emission detection configuration	
Spectral collection	300 to 810 nm
Spectral resolution	\leq 5 nm
SNR	\geq 200
Out-of band suppression of reflected light	\geq OD 5
Clinical operation	
Laparoscope compatibility	5 mm
Operating table compatibility	Yes
Single-site measurement time	Under 20 s
Dye delivery volume	1 μ L (\pm 1 nL)
Fiber optic probe	
Ovarian surface area in contact	1.6 mm ²
Approximate imaging depth	50 to 120 μ m
Sampling spot diameter	1 mm
Numerical aperture in tissue	0.17
Optical magnification	1

use, and the features of the fiber optic probe are listed in Table 4.

4 Discussion and Conclusion

We successfully designed and built a clinical research device for use intraoperatively to perform clinical measurements on ovaries, and we have successfully overcome the substantial challenges to implementation of a clinical intraoperative device.

In the design of the excitation light source, the light-leak in the near-infrared region for the selected 280-nm bandpass excitation filter (Semrock) is not critical, as the detection sensitivity is relatively low in that spectral region and data past 560 nm are excluded to avoid light at second order.

For the emission detection system, the first three long-pass filters (Chroma Technologies) have smoother spectral sensitivity values as compared to the last two (Omega Filters). This can be seen in Fig. 6. They differ due to differences in manufacturing techniques used. This is not a problem, as the short-

est period of the fluctuations is greater than 10 nm and is corrected using calibration. Also, this period is larger than the system resolution of 5 nm. The mismatch in the $F/\#$'s of the fiber and the detection optics that is causing 60% loss of collected emission light can be reduced by using a shorter focal length spectrometer. In addition, there is clipping of the fluorescence spectra at some excitation wavelengths, as seen in Fig. 9. Adopting a filter wheel with additional filter positions could extend the emission spectrum toward shorter wavelengths but is not feasible with the present spectrometer.

The issues with dye delivery cable length and hydrostatic pressure make the use of methylene blue as a marking dye somewhat ineffective, as we were not able to deliver a precise amount of dye over several meters of cable length. Surgical marking pens could be an alternative approach,^{36,37} but they are not yet approved for *in vivo* applications.^{33,38} The accuracy in locating the puncture sites might be improved with video recording of the measurement procedure, which might be more accurate than an anatomical sketch illustrating the loca-

tion of the measurement. The ideal length of the fiber optic probe would be 2 to 3 in longer than the present length of 14 in. The somewhat inadequate length of the probe in a large patient requires careful handling to keep the probe in constant contact with the ovary during a clinical measurement, which is a requirement for successful measurements.

The short-term fluctuations in power are not related to the long-term decrease in power due to lamp aging. They are due to warming-up of components in the light pathway and also due to small changes in the light-emitting plasma of the lamp's cloud, which could cause some arc-wander.³⁹ Power measurements during each exposure appear to be effective in cancelling those variations.

For the purpose of quality control of fluorescence measurements, the use of feedback fibers as well as an integrating sphere fiber is redundant. The excitation light is suppressed by the spectrometer's long-pass filters and cannot be measured during each sample exposure. Output of the excitation source is best monitored when the probe is placed into the integrating sphere and longpass filters are not engaged. However, for reflectance measurements, a spectral feedback measurement in combination with a sample measure has been shown to increase measurement precision.⁴⁰

When reviewing the calibration and quality control techniques in previous publications^{40–49} that deal with fluorescence spectroscopy to generate excitation–emission matrices, it was found that the techniques discussed here offer equal or better management. For instance, the Raman peak of water can be used to identify one peak emission wavelength. However, using around five or more peaks over the spectral range of interest provides better wavelength calibration. Spectral sensitivity calibration of the components of the system over the UV-visible spectrum needs at least two light sources having relatively flat spectra in the wavelength range of interest.

The results show that the CRD is capable of performing calibrated reliable and safe clinical measurements well within the time frame set by the IRB-approved research protocol. Performance of our system closely compares with that of an industry-standard bench-top device. In the future, the recorded data of our ongoing study will be statistically analyzed to determine the clinical efficacy in separating malignant growth from normal ovarian surface epithelium and to determine whether normal samples from patients at high risk differ from those at low risk for developing ovarian cancer. If proven effective, this technique could be useful for women requiring surveillance of their ovaries or as a follow-up test to other diagnostic techniques. For example, if ultrasound is used as the first diagnostic test, then optical spectroscopy could be used as the follow-up test to determine the need for ovary removal based on characteristics of malignancy. One potential limitation of this approach is the current paradigm shift that many of the cancers arise within the fallopian tube in patients with BRCA mutations.⁵⁰ However, there may be changes in the extracellular matrix (a field effect) in the ovary, as suggested with SHG of the ovary,^{51,52} which can be measured with fluorescence spectroscopy.

We have presented a potential approach that could also be adapted to transvaginal access, which would be less costly and less invasive. This approach, if proven effective, would be most useful and economical in women at high risk of de-

veloping ovarian cancer and might determine the ideal time for a high-risk woman to undergo an oophorectomy.

Acknowledgments

The authors wish to acknowledge the contribution of Rafal Pawluczyk, Kathy Schmidt, Moshe Zilversmit, Elias (Alex) Garcia, Glen Gerhard PhD, David Moore, Connie Moore, Nathaniel Kirkpatrick PhD, the surgical staff at UMC, the staff at the University Research Instrumentation Center (URIC), Timothy Renkoski, and Brenda Baggett. Rafal Pawluczyk from Fiber Tech Optica, Kitchener, Ontario, Canada, built the last two versions of the fiber optic probe. Kathy Schmidt was the research nurse. Moshe Zilversmit was associated with the development of the laparoscope adaptor used in the first generation of the fiber optic probe. Elias Garcia provided his expertise in cleaning and material selection for ETO sterilization of the fiber optic probe. Dr. Gerhard provided insights into the clinical engineering (CE) aspects of device development. The CRD was certified for clinical use by David Moore (CE) and Connie Moore (Infection Prevention and Epidemiology). Nathaniel Kirkpatrick, provided insights into some important areas of CRD and fiber optic probe development. The surgical staff provided valuable assistance in the clinical trials. Most custom mechanical components were manufactured by URIC. Timothy Renkoski and Brenda Baggett helped to review the manuscript. The authors thank the National Institutes of Health for funding this research through Grant No. CA098341.

References

1. G. D. Aletti, S. C. Dowdy, B. S. Gostout, M. B. Jones, R. C. Stanhope, T. O. Wilson, K. C. Podratz, and W. A. Cliby, "Quality improvement in the surgical approach to advanced ovarian cancer: the Mayo Clinic experience," *J. Am. Coll. Surg.* **208**(4), 614–620 (2009).
2. E. V. Bandera, L. H. Kushi, and L. Rodriguez-Rodriguez, "Nutritional factors in ovarian cancer survival," *Nutr. Cancer* **61**(5), 580–586 (2009).
3. A. Jemal, R. Siegel, E. Ward, Y. Hao, J. Xu, and M. J. Thun, "Cancer statistics, 2009," *Ca-Cancer J. Clin.* **59**(4), 225–249 (2009).
4. C. H. Holschneider and J. S. Berek, "Ovarian cancer: epidemiology, biology, and prognostic factors," *Semin Surg. Oncol.* **19**(1), 3–10 (2000).
5. D. A. Bell, "Origins and molecular pathology of ovarian cancer," *Mod. Pathol.* **18**(Suppl. 2), S19–32 (2005).
6. R. E. Scully, "Pathology of ovarian cancer precursors," *J. Cell Biochem. Suppl.* **23**, 208–218 (1995).
7. A. A. Tanbakuchi, A. R. Rouse, J. A. Udovich, K. D. Hatch, and A. F. Gmitro, "Clinical confocal microlaparoscope for real-time *in vivo* optical biopsies," *J. Biomed. Opt.* **14**(4), 044030 (2009).
8. D. Rabinerson, B. Kaplan, H. Levavi, and A. Neri, "The biology of ovarian cancer of epithelial origin," *Isr J. Med. Sci.* **32**(11), 1128–1133 (1996).
9. K. A. Baggerly, J. S. Morris, S. R. Edmonson, and K. R. Coombes, "Signal in noise: evaluating reported reproducibility of serum proteomic tests for ovarian cancer," *J. Natl. Cancer Inst.* **97**(4), 307–309 (2005).
10. W. Zhong, J. P. Celli, I. Rizvi, Z. Mai, B. Q. Spring, S. H. Yun, and T. Hasan, "*In vivo* high-resolution fluorescence microendoscopy for ovarian cancer detection and treatment monitoring," *Br. J. Cancer* **101**(12), 2015–2022 (2009).
11. N. Q. Nguyen, A. V. Biankin, R. W. Leong, D. K. Chang, P. H. Cosman, P. Delaney, J. G. Kench, and N. D. Merrett, "Real time intraoperative confocal laser microscopy-guided surgery," *Ann. Surg.* **249**(5), 735–737 (2009).
12. P. P. Provenzano, K. W. Eliceiri, and P. J. Keely, "Shining new light on 3D cell motility and the metastatic process," *Trends Cell Biol.* **19**(11), 638–648 (2009).

13. F. Collino, A. Revelli, M. Massobrio, D. Katsaros, M. Schmitt-Ney, G. Camussi, and B. Bussolati, "Epithelial-mesenchymal transition of ovarian tumor cells induces an angiogenic monocyte cell population," *Exp. Cell Res.* **315**(17), 2982–2994 (2009).
14. E. F. Petricoin, A. M. Ardekani, B. A. Hitt, P. J. Levine, V. A. Fusaro, S. M. Steinberg, G. B. Mills, C. Simone, D. A. Fishman, E. C. Kohn, and L. A. Liotta, "Use of proteomic patterns in serum to identify ovarian cancer," *Lancet* **359**(9306), 572–577 (2002).
15. R. C. Bast Jr., M. Brewer, C. Zou, M. A. Hernandez, M. Daley, R. Ozols, K. Lu, Z. Lu, D. Badgwell, G. B. Mills, S. Skates, Z. Zhang, D. Chan, A. Lokshin, and Y. Yu, "Prevention and early detection of ovarian cancer: mission impossible?," *Recent Results Cancer Res.* **174**, 91–100 (2007).
16. K. Maheedhar, R. A. Bhat, R. Malini, N. B. Prathima, P. Keerthi, P. Kushtagi, and C. M. Krishna, "Diagnosis of ovarian cancer by Raman spectroscopy: a pilot study," *Photomed. Laser Surg.* **26**(2), 83–90 (2008).
17. J. Q. Brown, K. Vishwanath, G. M. Palmer, and N. Ramanujam, "Advances in quantitative UV-visible spectroscopy for clinical and preclinical application in cancer," *Curr. Opin. Biotechnol.* **20**(1), 119–131 (2009).
18. S. G. Adie and S. A. Boppart, "Optical coherence tomography for cancer detection," in *Optical Imaging of Cancer*, E. Rosenthal and K. R. Kim, Eds., pp. 209–259, Springer, New York (2009).
19. C. L. Evans, I. Rizvi, T. Hasan, and J. F. de Boer, "In vitro ovarian tumor growth and treatment response dynamics visualized with time-lapse OCT imaging," *Opt. Express* **17**(11), 8892–8906 (2009).
20. Z. Yaqoob, J. Wu, E. J. McDowell, X. Heng, and C. Yang, "Methods and application areas of endoscopic optical coherence tomography," *J. Biomed. Opt.* **11**(6), 063001 (2006).
21. H. W. Wang, Y. H. Wei, and H. W. Guo, "Reduced nicotinamide adenine dinucleotide (NADH) fluorescence for the detection of cell death," *Anticancer Agents Med. Chem.* **9**(9), 1012–1017 (2009).
22. M. A. Brewer, K. Johnson, M. Follen, D. Gershenson, and R. Bast Jr., "Prevention of ovarian cancer: intraepithelial neoplasia," *Clin. Cancer Res.* **9**(1), 20–30 (2003).
23. M. Brewer, U. Utzinger, E. Silva, D. Gershenson, R. C. Bast Jr., M. Follen, and R. Richards-Kortum, "Fluorescence spectroscopy for in vivo characterization of ovarian tissue," *Lasers Surg. Med.* **29**(2), 128–135 (2001).
24. R. Richards-Kortum and E. Sevick-Muraca, "Quantitative optical spectroscopy for tissue diagnosis," *Annu. Rev. Phys. Chem.* **47**, 555–606 (1996).
25. J. R. Lakowicz, "Fluorophores," in *Principles of Fluorescence Spectroscopy*, J. R. Lakowicz, Ed., pp. 63–54, Kluwer Academic/Plenum Publishers, New York (1999).
26. M. A. Brewer, U. Utzinger, J. K. Barton, J. B. Hoying, N. D. Kirkpatrick, W. R. Brands, J. R. Davis, K. Hunt, S. J. Stevens, and A. F. Gmitro, "Imaging of the ovary," *Technol. Cancer Res. Treat.* **3**(6), 617–627 (2004).
27. American Conference of Government, Industry and Hygienists, in *2004 TLVs and BEIs: based on the documentation of the threshold limit values for chemical substances and physical agents and biological exposure indices ACGIH*, pp. 155–158, ACGIH Worldwide/Signature Publications, Cincinnati (2004).
28. E. V. S. Trujillo, D. R. Utzinger, U. Ramanujam, N. Mitchell, M. Follen, and R. Richards-Kortum, "Method to determine tissue fluorescence efficiency in vivo and predict signal-to-noise ratio for spectrometers," *Appl. Spectrosc.* **52**(7), 943–951 (1998).
29. U. Utzinger and R. R. Richards-Kortum, "Fiber optic probes for biomedical optical spectroscopy," *J. Biomed. Opt.* **8**(1), 121–147 (2003).
30. D. H. Wallace, M. G. Serpell, J. N. Baxter, and P. J. O'Dwyer, "Randomized trial of different insufflation pressures for laparoscopic cholecystectomy," *Br. J. Surg.* **84**(4), 455–458 (1997).
31. R. Kiesslich, J. Fritsch, M. Holtmann, H. H. Koehler, M. Stolte, S. Kanzler, B. Nafe, M. Jung, P. R. Galle, and M. F. Neurath, "Methylene blue-aided chromoendoscopy for the detection of intraepithelial neoplasia and colon cancer in ulcerative colitis," *Gastroenterology* **124**(4), 880–888 (2003).
32. A. Savitzky and M. J. E. Golay, "Smoothing and differentiation of data by simplified least-squares procedures," *Anal. Chem.* **36**, 1627–1639 (1964).
33. W. Au, M. A. Butler, S. E. Bloom, and T. S. Matney, "Further study of the genetic toxicity of gentian violet," *Mutat Res.* **66**(2), 103–112 (1979).
34. S. A. Prael, W. F. Cheong, and A. J. Welch, "A review of the optical properties of biological tissues," *IEEE J. Quantum Electron.* **26**, 2166–2185 (1990).
35. T. J. Farrell, M. S. Patterson, and B. Wilson, "A diffusion theory model of spatially resolved, steady-state diffuse reflectance for the noninvasive determination of tissue optical properties in vivo," *Med. Phys.* **19**(4), 879–888 (1992).
36. M. S. Granick, F. R. Heckler, and E. W. Jones, "Surgical skin-marking techniques," *Plast. Reconstr. Surg.* **79**(4), 573–580 (1987).
37. B. V. Stromberg, "The surgical marking pen: a comparative study," *Plast. Reconstr. Surg.* **80**(1), 104–107 (1987).
38. K. Brockow, P. Grabenhorst, D. Abeck, B. Traupe, J. Ring, U. Hoppe, and F. Wolf, "Effect of gentian violet, corticosteroid, and tar preparations in *Staphylococcus aureus*-colonized atopic eczema," *Dermatology* **199**(3), 231–236 (1999).
39. R. H. Breeze and B. Ke, "Some comments on xenon arc lamp stability," *Rev. Sci. Instrum.* **43**(5), 821–823 (1972).
40. B. Yu, H. Fu, T. Bydlon, J. E. Bender, and N. Ramanujam, "Diffuse reflectance spectroscopy with a self-calibrating fiber optic probe," *Opt. Lett.* **33**(16), 1783–1785 (2008).
41. C. Zhu, E. S. Burnside, G. A. Sisney, L. R. Salkowski, J. M. Harter, B. Yu, and N. Ramanujam, "Fluorescence spectroscopy: an adjunct diagnostic tool to image-guided core needle biopsy of the breast," *IEEE Trans. Biomed. Eng.* **56**(10), 2518–2528 (2009).
42. A. Baker, "Fluorescence excitation-emission matrix characterization of river waters impacted by a tissue mill effluent," *Environ. Sci. Technol.* **36**(7), 1377–1382 (2002).
43. R. D. JiJi, G. A. Cooper, and K. S. Booksh, "Excitation-emission matrix fluorescence based determination of carbamate pesticides and polycyclic aromatic hydrocarbons," *Anal. Chim. Acta* **397**(1–3), 61–72 (1999).
44. W. Chen, P. Westerhoff, J. A. Leenheer, and K. Booksh, "Fluorescence excitation-emission matrix regional integration to quantify spectra for dissolved organic matter," *Environ. Sci. Technol.* **37**(24), 5701–5710 (2003).
45. N. Patel-Sorrentino, S. Mounier, and J. Y. Benaïm, "Excitation-emission fluorescence matrix to study pH influence on organic matter fluorescence in the Amazon basin rivers," *Water Res.* **36**(10), 2571–2581 (2002).
46. J. Saurina, C. Leal, R. Compañó, M. Granados, R. Tauler, and M. D. Prat, "Determination of triphenyltin in sea-water by excitation-emission matrix fluorescence and multivariate curve resolution," *Anal. Chim. Acta* **409**(1–2), 237–245 (2000).
47. Y. Yan, H. Li, and M. L. Myrick, "Fluorescence fingerprint of waters: excitation-emission matrix spectroscopy as a tracking tool," *Appl. Spectrosc.* **54**(10), 1539–1542 (2000).
48. A. F. Zuluaga, U. Utzinger, A. Durkin, H. Fuchs, A. Gillenwater, R. Jacob, B. Kemp, J. Fan, and R. Richards-Kortum, "Fluorescence excitation emission matrices of human tissue: a system for in vivo measurement and method of data analysis," *Appl. Spectrosc.* **53**(3), 302–311 (1999).
49. R. A. Zangaro, J. Landulfo Silveira, R. Manoharan, G. Zonios, I. Itzkan, R. R. Dasari, J. V. Dam, and M. S. Feld, "Rapid multiexcitation fluorescence spectroscopy system for in vivo tissue diagnosis," *Appl. Opt.* **35**(25), 5211–5219 (1996).
50. P. A. Shaw, M. Rouzbahman, E. S. Pizer, M. Pintilie, and H. Begley, "Candidate serous cancer precursors in fallopian tube epithelium of BRCA1/2 mutation carriers," *Mod. Pathol.* **22**(9), 1133–1138 (2009).
51. N. D. Kirkpatrick, M. A. Brewer, and U. Utzinger, "Endogenous optical biomarkers of ovarian cancer evaluated with multiphoton microscopy," *Cancer Epidemiol. Biomarkers Prev.* **16**(10), 2048–2057 (2007).
52. O. Nadiamykh, R. B. LaComb, M. A. Brewer, and P. J. Campagnola, "Alterations of the extracellular matrix in ovarian cancer studied by second-harmonic generation imaging microscopy," *BMC Cancer* **10**, 94–108 (2010).